Analytical Methods

Accepted Manuscript

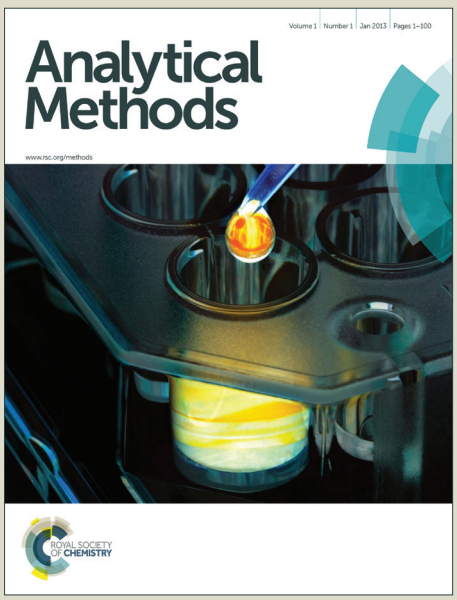

ROYAL SOCIETY OF CHEMISTRY

www.rsc.org/methods

Journal Name

RSCPublishing

ARTICLE

One-step synthesis of Pt-decorated graphene-carbon nanotube for electrochemical sensing of dopamine, uric acid and ascorbic acid

Cite this: DOI: 10.1039/x0xx00000x

Received ooth January 2012,

Accepted ooth January 2012

DOI: 10.1039/x0xx00000x

www.rsc.org/

S. Ramakrishnan[a,b], K. R.Pradeep[a], A. Raghul[a], R. Senthilkumar[a,b], Murali Rangarajan[a,b] and Nikhil K. Kothurkar[*a,b]

Platinum nanoparticle-decorated graphene and carbon nanotube nanocomposites (Pt-Gr-CNT) were synthesized by radio frequency chemical vapor deposition (RF-CVD) from ethanol, using a Pt/MgO catalyst. Morphological analysis showed Pt nanoparticles decorating graphene sheets and double-walled and multiwalled carbon nanotubes. It was observed that, upon encountering Pt nanoparticles, carbon nanotubes unravelled into graphene sheets. This may be due to graphitic carbon atoms from growing CNTs forming bonds with carbon atoms from other CNTs, particularly at the site of another Pt NP. The Pt-Gr-CNT-modified GCE showed high electrocatalytic activity towards the oxidation of ascorbic acid (AA), dopamine (DA) and uric acid (UA) in 0.1M phosphate buffer solution (pH 7.0) in cyclic voltammetry (CV) and differential pulse voltammetry (DPV) studies. CV showed well-separated oxidation peaks of AA (–99mV), DA (121mV) and UA (261mV). In DPV studies, the peak separation between AA-DA DA-UA and AA-UA were 210mV, 140mV and 360mV respectively. Simultaneous detection of AA, DA and UA using DPV, in respective concentration ranges of 200–900 μM, 0.2–30 μM, 0.1–50 μM, showed good linearity and sensitivities of 0.186 μA μM^{-1} cm^{-2} (AA), 9.199 μA $\mu M^{-1}cm^{-2}$ (DA) and 9.386 μA μM^{-1} cm^{-2} (UA) respectively. Pt-Gr-CNT/GCE was evaluated for simultaneous detection of the three biomolecules in real sample solutions of a vitamin C tablet, human serum and urine. It showed recoveries in the range of 93–101%, indicating that it is a promising platform for further biosensor development.

Introduction

Graphene (Gr) and its nanocomposites[1] have been used in numerous applications in various fields including solar energy,[2] electronics,[3] energy storage,[4] fuel cells,[5] and sensors.[6,7] It is well-known that graphene has large surface area, excellent electron mobility and conductivity, and wide electrochemical window.[8] On the other hand, there are many reports that pristine graphene may not exhibit substantial advantages as an electrode material, and that it is necessary to introduce structural defects or impurities (including the surfactants used in the synthesis) to achieve the desired functionality and electronic structure, and therefore enhanced electrochemical activity.[9] Using carefully constructed electrochemical experiments and density functional theory-based simulations, Brownson *et al*[10] demonstrated significant increase in the heterogeneous electron transfer rate (and thereby improved reversibility and catalytic activity) when the edge-to-basal plane ratio increased, viz., in few-layer graphene. The HOMO and LUMO of the graphene were found to be concentrated around the edges of the graphene sheets, validating the experimental observations. These results were similar to those observed in basal- and edge-plane graphite electrodes constructed from Highly Ordered Pyrolytic Graphite (HOPG).[11] Recently, few layer- to multilayer-graphene has shown better electrochemical activity with heterogeneous molecules.[12,13]

In addition to the above approach of using few-layer graphene as an electrode material, the electrocatalytic performance of graphene can also be improved by doping with heteroatoms such as nitrogen, boron or sulfur, which provide more active sites and tunability of the band gap.[14-16] Also, carbon nanomaterials (Gr and CNT) with metal or metal oxide nanoparticles (NPs) possess high electrocatalytic activity due to the increased number of active sites and improved selectivity.[17] Such systems provide a new avenue for fabricating sensors. The metal or metal oxide NPs can increase the electron transfer rate and improve the selectivity of the sensing electrodes due to

their differing interactions with different analytes. Electrodes with such modified graphene have been used for detecting various inorganic or organic electroactive compounds.[18,19]

Further, additional advantages can be derived by using NP-Gr-CNT three-component nanostructures. Lee *et al* have reported vertical N-doped carbon nanotube (VNCNT) arrays decorated with Au, Ru, or Mn nanoparticles on a graphene film and the field-emission properties of the nanostructures. The Mn-VNCNT field emitter showed the best performance among the emitters tested.[20] Yen *et al*. reported dye sensitized solar cells (DSSCs) containing TiO_2-Gr-CNT with a cell efficiency of 6.11%, which was 31% higher than that of conventional TiO_2 cell. The performance improvement was due to the presence of graphene and CNTs, where graphene provided a conductive pad with its large surface area, while the high aspect ratio of the CNTs connected the isolated graphene pads, yielding a more extensive conductive network in the composite working electrode.[21] Sun *et al* have reported a facile and green method to synthesize Pd nanoparticles (NPs) on a reduced graphene oxide (rGO)-CNT nanocomposite, which exhibited excellent and stable catalytic activity compared to other materials (Pd-rGO, Au/C core-shell).[19] Thus, NPs-Gr-CNT nanostructures are advantageous for electrochemical applications where the NPs provide the catalytic properties and the combination of Gr and CNT provides improved electron transfer to the electrode.[22-24] Most NPs-GR-CNT nanocomposites have been prepared by two- or three-step processes. Pt nanoparticles shows better electrocatalytic properties with graphene.[25,26] Biris *et al*. recently reported a one-step synthesis of Pt-Gr-CNT nanocomposite using methane as carbon precursor and studied the effect of the temperature, Pt:MgO ratio and methane flow rate on product morphologies.[27]

One of the important applications of such nanocomposites is in electrochemical sensors for analytes such as dopamine (DA), ascorbic acid (AA) and uric acid (UA). These biomolecules are important compounds of the human body, playing important roles in the human metabolism, central nervous and renal systems. DA plays a major role in the proper functioning of central nervous, renal, hormonal and cardiovascular systems.[28] AA plays an important role in many biological processes such as cancer prevention and immunity improvement.[29] Uric acid is the end product of the catabolism of purine nucleosides. An elevated level of uric acid in the blood is clinically pertinent to gout, renal failure, leukemia and lymphoma.[30] AA usually coexists with DA in extracellular fluid; UA and AA co-exist in blood and urine. Using a bare carbon electrode, DA, AA and UA are oxidized at practically the same potential, with relatively low currents. Thus, there is both poor selectivity and poor sensitivity. It is necessary to develop a simple, fast, selective and sensitive method for the simultaneous sensing of AA, DA and UA. Simultaneous electrochemical detection of DA, AA and UA has been reported using electrochemical reduced graphene oxide,[31] NPs (Pt, Au, Ag, metal oxides), Gr, functionalized-Gr,[32-36] and NPs-Gr.[37]

We report the simultaneous detection of DA, AA and UA using a Pt-Gr-CNT nanocomposite synthesized by a one-step RF-CVD synthesis using ethanol as the carbon source. The composite clearly showed Pt nanoparticles, double-walled and multiwalled carbon nanotubes (DWCNT) and multi-layer graphene and was able to simultaneously detect AA (50 μM), DA (0.01 μM), and UA (0.1 μM).

Experimental

Materials

Magnesium oxide (MgO) and chloroplatinic acid were purchased from Sigma Aldrich. Ethanol and hydrochloric acid used were of lab grade. Pure dopamine, ascorbic acid and uric acid were purchased from Sigma Aldrich. For real sample analysis, a commercially available vitamin C tablet IP500mg (Celin®) was used. Human serum and urine were obtained from the Diagnostic Centre, Shanthi Social Services, Coimbatore, Tamil Nadu, India, with informed consent of the subjects. This research was conducted with the approval of the University Ethics Committee of Amrita Vishwa Vidyapeetham and was in compliance with the relevant laws and the University's guidelines.

Preparation of catalyst: Pt/MgO

MgO (300mg) was dissolved in 10 mL ethanol and sonicated for 1 hour. $PtHCl_6.6H_2O$ (84.9 mg; 2% Pt loading) was also dissolved in 10 mL ethanol. The platinum precursor and MgO solutions were mixed and sonicated for another 1 hour and stirred overnight. The solvent was evaporated in a rotary evaporator and the obtained powder was calcined in a muffle furnace at 500°C for an hour. After calcination the final sample weighed around 295.5 mg. This catalyst was used for the synthesis of Pt-Gr-CNT.

Synthesis of Pt-Gr-CNT

About 100 mg of the prepared catalyst was uniformly spread as a thin layer on a graphite boat (susceptor) and placed at the center of a 2 inch diameter-quartz tube. The quartz tube was purged with 400 mL/min of argon gas and heated using RF heating to 1000°C. Ethanol was introduced at 2 mL/hour for about 30 min at the reaction temperature of 1000°C. After flushing the system with argon, the reaction product (120.3 mg) was collected from the graphite boat and purified with dil. HCl. 76mg of purified product (Pt-Gr-CNT) was obtained.

Preparation of Pt-Gr-CNT/GCE

Glassy carbon electrode (GCE) was activated by polishing with different grades of silica slurry ranging from 0.05μ–3.00μ on a synthetic cloth and rinsing with ultrapure Millipore water. Pt-Gr-CNT nanocomposite (5 mg) was dispersed in 5 ml ultrapure Millipore water. About 20 μL of Pt-Gr-CNT nanocomposite solution was placed on the pre-polished GCE and dried at 70°C overnight.

Characterization

Scanning electron microscopy was carried out by SEM (VEGA 3 Tescan) with EDAX (Bruker). High resolution transmission electron microscopy (HRTEM) analysis was carried out using a JEOL JEM 2100 transmission electron microscope. Raman spectroscopy was carried out using confocal micro-Raman spectrometer (Renishaw RM 2000; Ar^+ laser of 514 nm). X-ray diffraction was carried out on a Rigaku Miniflex 600 model. Electrochemical experiments were carried out on a standard three-electrode system using a WaveNow potentiostat (Pine Instruments) with GCE as working electrode, platinum wire (CH Instruments) as an auxiliary electrode, and Ag/AgCl (3 M KCl; CH Instruments) as the reference electrode.

Results and Discussions

Materials Characterization

Figure 1(a-b) shows flake-like structures made out of stacks of wrinkled graphene sheets of sizes on the order of a few microns. Figure 1(c) shows the EDAX spectrum of Pt-Gr-CNT nanocomposite, which indicates the presence of Pt. The Raman spectrum of graphene is characterized by two prominent features: a G-band at 1567 cm^{-1} arising due to the first order Raman scattering of the E_{2G} phonon at the Brillouin zone center of sp^2 carbon atoms and a D-band arising from the breathing mode of the K-point phonons of A_{1G} symmetry at 1356 cm^{-1}. The D-band requires a defect for its activation and hence, it acts as an indicator of defects. Figure 2(a) indicates the 2D, G and D bands with peak positions at 2672 cm^{-1}, 1582 cm^{-1} and 1336 cm^{-1} respectively. An intensity ratio of the G and D bands (I_G/I_D) equal to 0.95 indicates a more defective graphene, due to the presence of Pt nanoparticles, as compared to pristine graphene ($I_G/I_D \geq 1$).

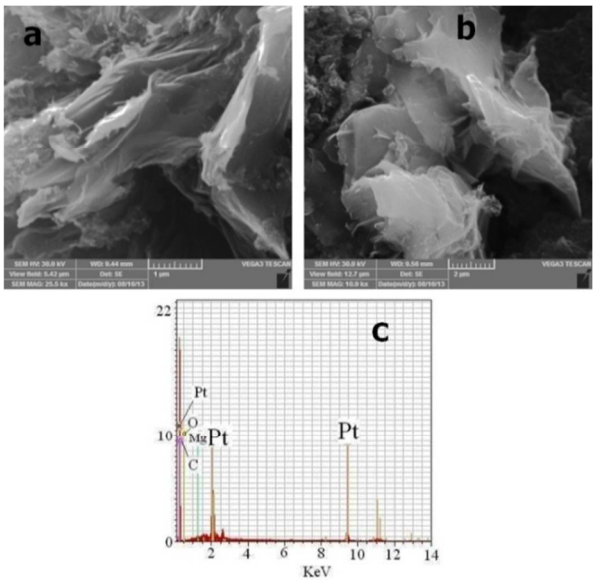

Figure 1: SEM images (a-b) and EDX spectrum (c) of Pt-graphene-CNT

The full width at half maximum (FWHM) values of the 2D band is 107cm^{-1}, which indicates the presence of multilayer graphene.[38] Figure 2(b) shows the XRD spectrum of the Pt-Gr-CNT nanocomposite, with a peak at 2θ values of 26.5°, which belongs to (200) plane of graphitic carbon. The strong diffraction peaks from Pt at 2θ values of 39.7°, 46.2°, 67.5° and 81.1° corresponding to the crystal planes (111), (200), (220) and (311) respectively, are in a good agreement with FCC Pt (JCPDS 87-0647). Figure 3(a-d) shows TEM images of the Pt-Gr-CNT nanocomposite. Figures 3a and 3b show the presence of graphene, along with CNTs and Pt nanoparticles. Figure 3(a) inset shows roughly 15–20 layers of graphene. Double-walled carbon nanotubes are clearly visible in Figure 3(c) and Pt-nanoparticles are distributed on the graphene-CNT. Figure 3(d) shows Pt-nanoparticles on the Gr-CNT with a d-spacing of 0.22nm (inset), corresponding to the (111) plane. The majority of the Pt-nanoparticles were 4–8nm in size (Figure 3e).

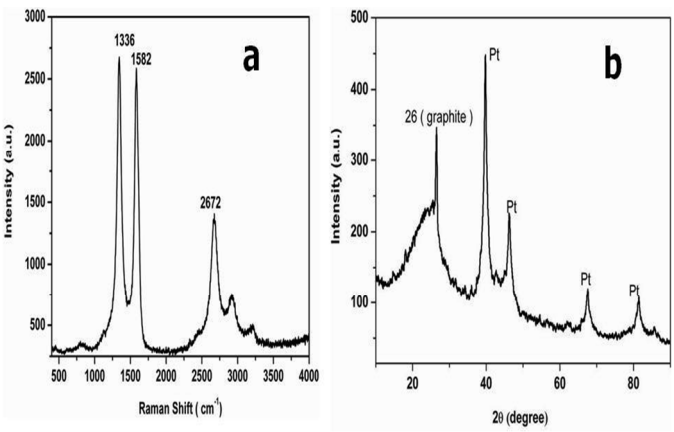

Figure 2: Raman spectra (a) and XRD (b) of Pt-graphene-CNT composite

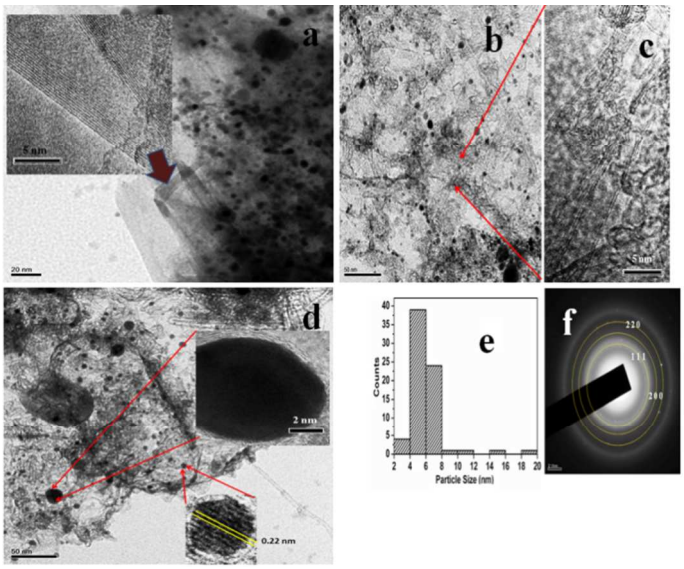

Figure 3: TEM images of Pt-graphene-CNT (a, b, d) and with Pt-decorated double walled carbon nanotubes and graphene (c). Histogram of particle size distribution of Pt nanoparticles (e), SAED pattern of Pt-graphene-CNT (f).

The SAED pattern (Figure 3f) shows diffraction rings corresponding to the (111), (200) and (220) planes with d-spacings of 0.22, 0.19 and 0.13 nm respectively, which is agreement with XRD and TEM results. The TEM image (Figure 3d (insert)) shows a graphene layer encapsulating a Pt NPs. Figure 4(a-b) TEM images of Pt-Gr-CNT (square and circle) show a DWCNT, which has got unrolled to become a graphene sheet after encountering a Pt NP. This gives an insight into the formation of the observed morphology of the material, where multilayer of graphene sheets are formed along with CNTs and Pt NPs. Pt NPs are known to be catalysts for CNT growth. The graphitic carbon atoms from growing CNTs can form bonds with carbon atoms from other CNTs, particularly at the site of another Pt NPs (Figure 4(a-b) red color indicators). This leads to the opening up of the CNT and the formation of graphene sheets.[39,40]

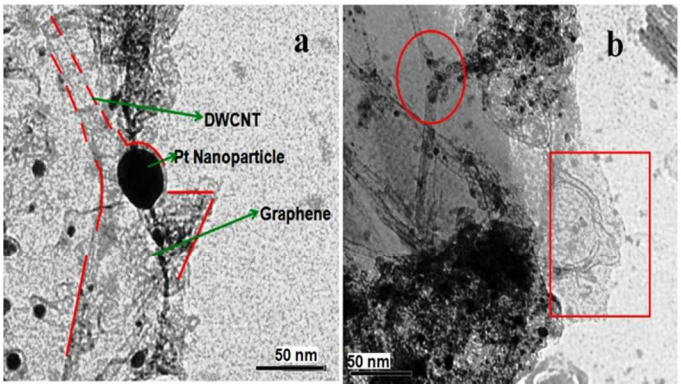

Figure 4: TEM images of Pt-Gr-CNT. Double-walled CNT, (marked with a red dotted line) getting unrolled to form graphene, at the location of a Pt particle. (a). Similar unrolling of CNTs found at Pt particles in the circular and square areas marked in red (b).

Electrochemical characterization of bare GCE and Pt-Gr-CNT/GCE

Figure 5(a) shows the cyclic voltammograms of bare GCE (black) and GCE with Pt-Gr-CNT (Pt-Gr-CNT/GCE). In order to find the peak current of the electrodes, CVs were conducted in 0.10M PBS (pH 7.). Figure 5(a) shows the CV curves of the bare GCE and Pt-Gr-CNT/GCE. Pt-Gr-CNT/GCE shows much higher peak currents compared to bare GCE, due to the increased surface area of the modified electrode. Pt-Gr-CNT electrode [surface area: 0.18 cm^2, see Supplementary Information] has about four times higher area than GCE [surface area: 0.048 cm^2]. In Figures 5(b-d), AA and UA show irreversible oxidation peaks and DA shows quasi-reversible electrochemical behaviour on bare GCE and Pt-Gr-CNT/GCE. Figure 5(b) shows the CV curves of GCE and Pt-Gr-CNT/GCE in 1mM of AA acid in 0.1M PBS pH 7.0. The former shows an oxidation peak at 417mV with a corresponding current of 13µA. Pt-Gr-CNT/GCE, on the other hand, shows an oxidation peak at 167mV with a corresponding current of 84.72 µA. Figure 5(c) shows the CV curves of GCE and Pt-Gr-CNT/GCE modified electrode in 0.5mM of DA acid in 0.1M PBS (pH 7.0). Bare GCE shows an oxidation peak at 184mV with current of 12.9µA and reduction peak at 56mV with current of −1.568 µA. On the other hand, Pt-Gr-CNT/GCE shows an oxidation peak at 176mV with corresponding peak current of 84 µA and reduction peak at 125mV with a peak current of −36.89µA. Figure 5(d) shows the CV curves of GCE and Pt-Gr-CNT/GCE of 0.5mM of UA acid in 0.1M PBS (pH 7.0). Bare GCE shows an oxidation peak at 397mV and current 10.52µA. Pt-Gr-CNT/GCE shows an oxidation peak at 302mV and current peak at 79.0 µA.

We observed that Pt-CNT-Gr/GCE shows enhanced peak current of analytes (AA, DA and UA) compared to reported values.[41,42] Figures 5(b-d) reveals the oxidation peaks of AA, DA and UA which are negatively shifted and their oxidation peak current increased with Pt-Gr-CNT/GCE. These indicate significant catalytic activity of the Pt-Gr-CNT/GCE.[43]

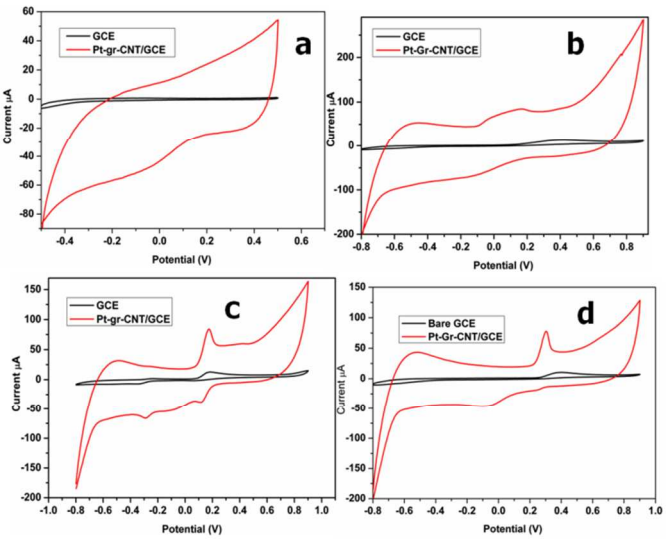

Figure 5: Cyclic voltammograms using glassy carbon electrode and glassy carbon electrodes with Pt-Gr-CNT in (a) 0.1M phosphate buffer solution (PBS) at pH 7.0) (b) 1mM of ascorbic acid in PBS (c) 500µM of dopamine in PBS (d) 500 µM of uric acid in PBS.

Studies were also conducted for selective determination of DA, UA and AA. Figure 6 (a) shows the CV curve of bare GCE (black colour) and Pt-Gr-CNT/GCE (red colour) 0.5M of AA, 100 µM of DA and UA in 0.1M (pH 7.0) in PBS solution. The bare GCE shows only two oxidation peaks at 139mV and 269 mV, which correspond to DA and UA, respectively. The oxidation peak of AA is not clearly observed. The Pt-Gr-CNT /GCE, on the other hand, reveals well separated oxidation peaks at −40mV, 168mV and 302mV corresponding to AA, DA and UA respectively. The oxidation peak separation between AA and DA is 208 mV and oxidation peak separation between DA-UA is 134mV. This is a good indication of the ability of thPt-Gr-CNT/GCE to selectively and simultaneously determine DA,UA and AA. Figure 6(b) shows the DPV curve of GCE and Pt-Gr-CNT/GCE in 0.5mM of AA, 100µM of DA and 100µM of UA in 0.1M PBS (pH 7.0). The oxidation peaks are

overlapped with bare GCE, which shows inability in distinguishing the molecules (AA, DA and UA). The corresponding DPV of Pt-Gr-CNT modified electrode (Figure 6(b) red colour) shows well-separated oxidation with peaks of AA (–99mV), DA (121mV) and UA (261mV), and peak separation between AA-DA DA-UA and AA-UA being 210mV, 140mV and 360mV respectively.

These results suggest that the electron transfers for the oxidation of AA, DA and UA at the Pt-Gr-CNT nanocomposite are much easier, due to the increased surface area and catalytic activity. Such an improvement in electron transfer kinetics could be attributed to movement of electrons from graphene to carbon nanotube, which are favorable sites for transferring the electrons, and we believe Pt nanoparticles accelerate the electron transfer between electrode surface and electroactive molecules.

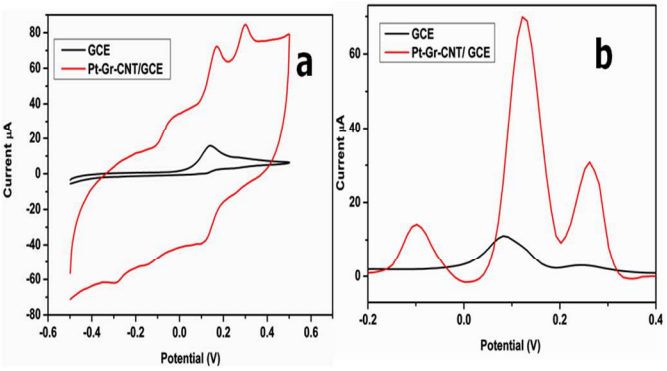

Figure 6: Cyclic voltammograms in a solution containing 500µM of ascorbic acid (AA), 100 µM of dopamine (DA) and uric acid (UA) in 0.1 M PBS (pH 7.0), using GCE and Pt-Gr-CNT/GCE electrodes and (b) Differential pulse voltametry curves in a solution containing 500 µM of ascorbic acid and 100µMof dopamine and uric acid in 0.1M PBS (pH 7.0), using GCE and Pt-Gr-CNT/GCE electrodes

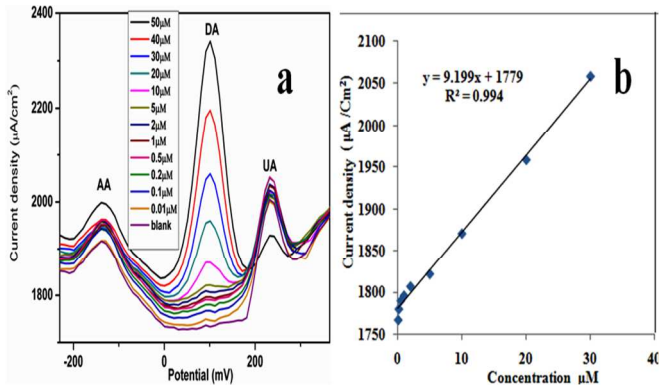

Figure 7: Differential pulse voltammetry curves in a solution containing 0.5mM of ascorbic acid and 20µM of uric acid with different concentrations (0.2 - 30 µM) of dopamine (a) and the linear fit of concentration vs. peak current density (b).

Since differential pulse voltammetry (DPV) has much higher current sensitivity and better resolution than cyclic voltammetry, it was used in the oxidation of AA, DA and UA in a mixture. Figure 7(a) shows DPV of various concentrations of DA in the presence 0.5mM of AA and 20µM of UA at Pt-Gr-CNT/GCE. Dopamine was detected in the range of 0.01 µM–50 µM in the presence of constant concentration of AA and UA in PBS (pH 7.0). The calibration plot of current density (µA/cm^2) versus concentration (µM) of DA (Figure 7(b)) shows a linear range of 0.2 µM–30 µM with R^2 = 0.994. The sensitivity of Pt-Gr-CNT/GCE with DA was 9.199 µA µM^{-1} cm^{-2} and the detection limit was 0.01 µM. Figure 8(a) shows DPV of various concentrations of UA in the presence of 0.5mM of AA and 10µM of DA in 0.1M PBS (pH 7.0). The plot of peak current density (µA/cm^2) vs concentration of UA (µM) indicates (Figure 8(b)) a linear behavior in the range 0.1-50µM with R^2 = 0.993. The sensitivity of Pt-Gr-CNT/GCE with UA was 9.386 µA µM^{-1} cm^{-2} and detection limit 0.1 µM. Figure 9(a) shows the DPV of various concentrations of AA in the presence of 10µM of DA and UA in 0.1M PBS (pH 7.0). The concentration of AA was varied from 200 µM to 900 µM. The calibration plot shows (Figure 9(b)) linear behavior in the range of 200-900 µM with R^2 = 0.997.The sensitivity of Pt-Gr-CNT/GCE with AA was 0.186 µA µM^{-1} cm^{-2} and detection limit was 50 µM.

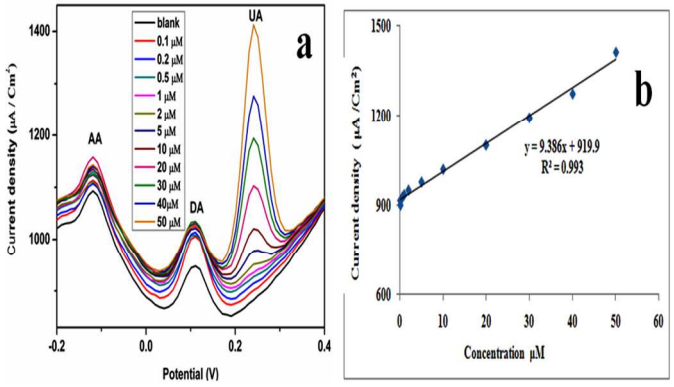

Figure 8: Differential pulse voltammetry curves in a solution containing 0.5mM of AA and 20µM of DA with different concentrations of uric acid (0.1–50 µM) of uric acid (a) and the linear fit of concentration vs. peak current density.(b).

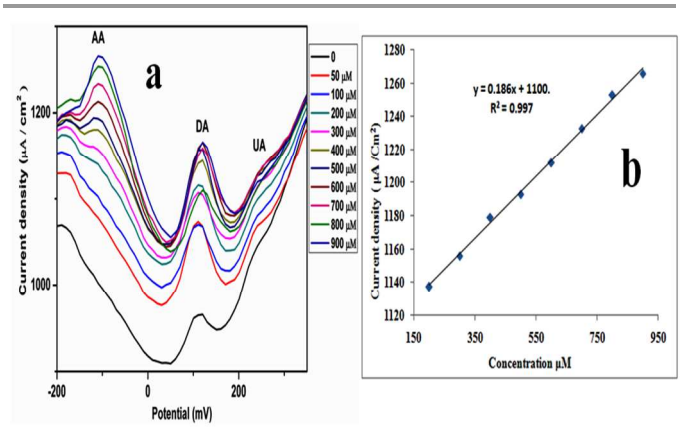

Figure 9: Differential pulse voltammetry curves in a solution containing 10µM of dopamine and uric acid with different concentrations of AA (50–900 µM) of ascorbic acid (a) and the linear fit of concentration (200–900 µM) vs. peak current density (b).

Table 1 compares the results of several reports of Pt-graphene-based, simultaneous electrochemical sensing of AA, DA and UA, with the present work. It is quite clear that the Pt-CNT-Gr/GCE electrode shows better peak separation between AA, DA and UA than the compared reports.[35-37,42]

Table1: Comparison of simultaneous electrochemical sensing of ascorbic acid, dopamine and uric acid using platinum-graphene-based materials

Materials	Methods	Linear range (μM)			Detection limit (μM)			Peak separation (mV)		
		AA	DA	UA	AA	DA	UA	AA-DA	DA-UA	AA-UA
Pt/Pd doped Gr[37]	DPV	40-1200	4-200	4-400	0.61	0.04	0.1	184	116	300
CS-Gr[36]	DPV	50-1200	1.2-24	2-45	50	1	2	165	90	225
Pt-MWCNT/GCE [42]	DPV	24.5-765	0.01-2.03	0.46-50	20	0.04	0.35	166	120	286
Gr /Pt/GCE[35]	DPV & AM	0.15-34.4	0.03-8.13	0.05-11.85	0.15	0.03	0.05	185	144	329
Pd/Gr/CS GCE [44]	DPV	100-4000	0.5-15 & 20-200	0.5-200	20	0.1	0.17	252	144	396
EC-RGO /GCE[45]	DpV	500-2000	0.5–60	0.5–60	250	0.5	0.5	240	130	NA
Pt/RGO/GCE[41]	DPV	NA	10-170	10-130	NA	0.25	0.45	NA	163	NA
Pt-CNT-GR/GCE (Present work)	DPV	200-900	0.1-30	0.1-50	50	0.01	0.1	208	140	360

CS- Chitosan: EC electrochemical: AM-amperometric: NA-data not available

Table 2: Determination of AA, DA and UA in real samples (serum, urine andvitamin C tablet). Values in parentheses are standard deviations of 3 samples

Samples	Detected (μM)			Added (μM)			Detected after addition (μM)			Recovery % (standard deviation)		
	P			**Q**			**R**			**100x (R-P)/Q**		
	AA	DA	UA	AA	DA	UA	AA	DA	UA	AA	DA	UA
Serum	-	30.77	12.83	-	40	50	-	70.61	59.94	-	99.80(0.84)	94.22(4.73)
	-	-	-	-	50	70	-	81.60	83.39	-	101.67(3.70)	100.80(5.19)
Urine	518	-	22	400	-	40	912.92	-	59.66	100.16(3.22)	-	94.16 (3.81)
	-	-	-	600	-	50	1140.0	-	70.33	101.44(3.84)	-	96.66 (5.03)
Vitamin C (tablet)	978.22	-	-	300	-	-	1265.5	-	-	95.83(2.59)	-	-
	-	-	-	400	-	-	1353.5	-	-	93.87(6.18)	-	-

Journal Name

RSCPublishing

ARTICLE

In the case of AA, the linear range of Pt-CNT-Gr/GCE is somewhat smaller than that of other reports but there is an overlap between the linear range and (200-900μM) and the normal range expected in urine. The normal range of AA levels in serum, falls below the linear range tested in this study. The linear range of Pt-CNT-Gr/GCE for sensing dopamine, while not the widest among the literature reports, is wider than the normal levels found in human urine. The lower detection limit of this material is also lower than the normal level in urine. As far as the dopamine levels in blood (pico molar) are concerned, none of the compared materials are satisfactory. For uric acid, of Pt-CNT-Gr/GCE, along with the report of Yan *et al*.[37] show the lowest detection limit. The linear range is comparable or superior to most other reports, however, considering the normal levels of UA in blood, the results of Yan *et al*. [37] might be more suitable.

To estimate the reproducibility of the Pt-CNT-graphene-modified electrode, five electrodes were prepared independently. The relative standard deviations (% RSD) in the measurements of the oxidation peak currents in DPV for 1000μM of AA, 50 μM DA and 50 μM UA for the five electrodes were found to be 6.7%, 7.1%, and 8.6 % respectively, indicating good reproducibility.

To determine the repeatability of the Pt-CNT-Gr/GCE for simultaneous detection of AA, DA and UA, the oxidation peak currents (DPV) were measured for a solution containing 1000 μM AA, 50 μM of DA and 50 μM UA using the Pt-CNT-Gr/GCE for 10 successive runs. The relative standard deviations (RSD) for the oxidation peak currents of AA, DA and UA for the 10 successive runs were 1.7%, 1.9% and 3.2% for AA, DA and UA, respectively, indicating excellent reproducibility of the Pt-CNT-Gr/GCE.

Stability of Pt-Gr-CNT/GCE electrode:

The storage stability of Pt-CNT-Gr /GCE was also evaluated by comparing the oxidation peak currents for AA, DA and UA from solution containing 1000 μM AA, 50 μM of DA and 50 μM UA after a period of 12 days. The deviations in the DPV peak oxidation currents were -9.21% for AA, -7.60% for DA and -8.10% for UA. The results indicate the excellent stability over the short term. Long term storage stability will be investigated in the future.

Real Samples Analysis

Determination of the concentrations of AA, DA, UA in real samples was performed by DPV using the Pt-Gr-CNT /GCE. For the real sample analyses, a commercially available Vitamin C tablet, and samples of human serum and urine were used. To prepare the solutions, 50mg of Vitamin C tablet powder, 0.5ml of serum and 0.5 ml urine were dissolved separately in 0.1M PBS to make 100 ml of each solution. The concentrations of AA, DA, UA in each of the real sample solutions were measured using Pt-Gr-CNT/GCE by DPV. Then known amounts of AA, DA and UA were added to the solutions and the AA, DA and UA concentrations in them were again measured. The measurements are summarized in Table 2. The recovery calculated as indicated in Table 2, was found to be in the range of 93.87–101.67% with a standard derivation of less than 6.1%. The high recovery values indicate good performance of Pt-Gr-CNT/GCE even for real samples.

Conclusion

We have demonstrated a one-step synthesis of Pt-decorated graphene-carbon nanotube nanomaterial (Pt-Gr-CNT) made by RFCVD using ethanol as the carbon precursor. Ethanol, due to the presence of oxygen, can oxidize the amorphous carbon formed during synthesis, thereby increasing the crystallinity of the material. HRTEM images show the presence of DWCNT and multilayer graphene decorated with Pt nanoparticles of sizes 4–8nm. The Pt-Gr-CNT obtained was used for the detection of biological molecules. We have demonstrated the simultaneous detection of ascorbic acid (AA), dopamine (DA) and uric acid (UA) using 0.1M PBS (pH = 7.0) since there is good separation between the respective peak potentials and good sensitivities, 9.199 μA μM^{-1} cm^{-2} (DA) and 9.386 μA μM^{-1} cm^{-2} (UA), respectively. Pt-Gr-CNT also showed low detection limits for the three biomolecules: 50 μM (AA), 0.01 μM (DA) and 0.1 μM (UA). The sensor shows excellent linearity in the ranges 0.1–50 μM for UA, 0.2–30 μM for DA, and 200–900 μM for in solutions containing all three biomolecules simultaneously. Real sample analysis conducted on samples of commercially available Vitamin C tablets, human serum and urine, showed recovery in the range of 93–101% indicating that Pt-Gr-CNT is a promising platform for simultaneous detection of biomolecules.

Acknowledgements

The authors thank DRDO, India for funding this research. Thanks are due to Mr. Vijayaraghavan Thiruvenkatam, PSG Institute of Advanced Studies for assistance in HRTEM analysis and Dr. Vijayalakshmi, Head-Diagnostic Centre, Shanthi

Social Services, Coimbatore-641 005 for her help in obtaining samples for real sample analysis.

Notes

[a]Center of Excellence in Advanced Materials and Green Technologies, Amrita Vishwa Vidyapeetham University, Coimbatore-641112

[b]Department of Chemical Engineering and Material Science, Amrita Vishwa Vidyapeetham University, Coimbatore-641112

Electronic Supplementary Information (ESI) available: See
DOI: 10.1039/b000000x/

References

1. S. Ramakrishnan, M. Dhakshnamoorthy, E. J. Jelmy, R. Vasanthakumari and N. K. Kothurkar, *RSC Adv*, 2014, **4**, 9743-9749.
2. X. Wang, L. Zhi and K. Mullen, *Nano Lett.*, 2007, **8**, 323-327.
3. S. Y. Jeong, S. H. Kim, J. T. Han, H. J. Jeong, S. Y. Jeong and G.-W. Lee, *Adv. Funct. Mater.*, 2012, **22**, 3307–3314.
4. S. Li, Y. Luo, W. Lv, W. Yu, S. Wu, P. Hou, Q. Yang, Q. Meng, C. Liu and H.-M. Cheng, *Adv. Energy Mater*, 2011, **1**, 486–490.
5. Z. Yao, M. Zhu, F. Jiang, Y. Du, C. Wang and P. Yang, *J. Mater. Chem.*, 2012, **22**, 13707-13713.
6. T. Qian, C. Yu, X. Zhou, S. Wu and J. Shen, *Sensor Actuat. B-Chem*, 2014, **193**, 759-763.
7. D. A. C. Brownson and C. E. Banks, *Analyst*, 2011, **136**, 2084-2089.
8. C. N. R. Rao, K. Biswas, K. S. Subrahmanyam and A. Govindaraj, *J. Mater. Chem.*, 2009, **19**, 2457-2469.
9. D. A. C. Brownson, D. K. Kampouris and C. E. Banks, *Chem. Soc. Rev.*, 2012, **41**, 6944-6976.
10. D. A. C. Brownson, L. J. Munro, D. K. Kampouris and C. E. Banks, *RSC Adv*, 2011, **1**, 978-988.
11. D. A. C. Brownson, S. A. Varey, F. Hussain, S. J. Haigh and C. E. Banks, *Nanoscale*, 2014, **6**, 1607-1621.
12. E. P. Randviir, D. A. C. Brownson, M. Gomez-Mingot, D. K. Kampouris, J. Iniesta and C. E. Banks, *Nanoscale*, 2012, **4**, 6470-6480.
13. E. P. Randviir, D. A. C. Brownson, J. P. Metters, R. O. Kadara and C. E. Banks, *Phys Chem Chem Phys*, 2014, **16**, 4598-4611.
14. P. Guo, F. Xiao, Q. Liu, H. Liu, Y. Guo, J. R. Gong, S. Wang and Y. Liu, *Sci. Rep.*, 2013, **3**, 03499.
15. S. Cui, S. Mao, G. Lu and J. Chen, J. Phys. Chem. Lett, 2013, **4**, 2441-2454.
16. P. Xu, D. Wu, L. Wan, P. Hu and R. Liu, *J. Colloid Interface Sci.*2014, **421**, 160-164.
17. F. M. Z. H. Song Yingpan, *Prog Chem*, 2012, 1665-1673.
18. D. A. C. Brownson and C. E. Banks, *RSC Adv*, 2012, **2**, 5385-5389.
19. T. Sun, Z. Zhang, J. Xiao, C. Chen, F. Xiao, S. Wang and Y. Liu, *Sci. Rep.*, 2013, **3**, 2527.
20. D. H. Lee, J. A. Lee, W. J. Lee, D. S. Choi, W. J. Lee and S. O. Kim, *J. Phys. Chem. C*, 2010, **114**, 21184-21189.
21. M.Y. Yen, M.C. Hsiao, S.H. Liao, P.-I. Liu, H.M. Tsai, C.C. M. Ma, N.-W. Pu and M.-D. Ger, *Carbon*, 2011, **49**, 3597-3606.
22. Q. Su, Y. Liang, X. Feng and K. Mullen, *Chem. Commun.*, 2010, **46**, 8279-8281.
23. D. Cai, M. Song and C. Xu, *Adv. Mater.*, 2008, **20**, 1706-1709.
24. Z. Fan, J. Yan, L. Zhi, Q. Zhang, T. Wei, J. Feng, M. Zhang, W. Qian and F. Wei, *Adv. Mater.*, 2010, **22**, 3723-3728.
25. D. Bin, F. Ren, H. Wang, K. Zhang, B. Yang, C. Zhai, M. Zhu, P. Yang and Y. Du, *RSC Adv*, 2014, **4**, 39612-39618.
26. Q. Zhang, F. Jiang, R. Yue and Y. Du, *RSC Adv,* 2014, **4**, 12105-12108.
27. A. R. Biris, M. D. Lazar, S. Pruneanu, C. Neamtu, F. Watanabe, G. K. Kannarpady, E. Dervishi and A. S. Biris, *RSC Adv*, 2013, **3**, 26391-26402.
28. A. Liu, I. Honma and H. Zhou, *Biosens.Bioelectron*, 2005, **21**, 809-816.
29. G.-C. Yen, P.D. Duh and H.L. Tsai, Food *Chem*, 2002, **79**, 307-313.
30. V. V. S. E. Dutt and H. A. Mottola, *Anal. Chem.*, 1974, **46**, 1777-1781.
31. H. Wang, F. Ren, C. Wang, B. Yang, D. Bin, K. Zhang and Y. Du, *RSC Adv*, 2014, **4**, 26895-26901.
32. L. Tan, K. G. Zhou, Y. H. Zhang, H. X. Wang, X. D. Wang, Y. F. Guo and H. L. Zhang, *Electrochem commun.*, 2010, **12**, 557-560.
33. Mouhong Lin, Haoliang Huang, and Yingju Liu, Canjian Liang, Shidong Fei, Xiaofen Chen and C. Ni., *Nanotechnology*, 2013, **24**, 065501.
34. J. Du, R. Yue, F. Ren, Z. Yao, F. Jiang, P. Yang and Y. Du, *Gold Bulletin*, 2013, **46**, 137-144.
35. C.-L. Sun, H.-H. Lee, J.-M. Yang and C.-C. Wu, *Biosens.Bioelectron*, 2011, **26**, 3450-3455.
36. D. Han, T. Han, C. Shan, A. Ivaska and L. Niu, *Electroanalysis*, 2010, **22**, 2001-2008.
37. J. Yan, S. Liu, Z. Zhang, G. He, P. Zhou, H. Liang, L. Tian, X. Zhou and H. Jiang, *Colloids Surf B Biointerfaces*, 2013, **111**, 392-397.
38. A. C. Ferrari, J. C. Meyer, V. Scardaci, C. Casiraghi, M. Lazzeri, F. Mauri, S. Piscanec, D. Jiang, K. S. Novoselov, S. Roth and A. K. Geim, *Phys. Rev.Lett.*, 2006, **97**, 187401.
39. D. Ding, Z.-L. Song, Z.-Q. Cheng, W.-N. Liu, X.-K. Nie, X. Bian, Z. Chen and W. Tan, *J. Mater. Chem. A*, 2014, **2**, 472-477.

40. Y. Mizutani, N. Fukuoka, S. Naritsuka, T. Maruyama and S. Iijima, *Diam. Relat. Mater*, 2012, **26**, 78-82.

41. T. Q. Xu, Q. L. Zhang, J. N. Zheng, Z. Y. Lv, J. Wei, A. J. Wang and J. J. Feng, *Electrochim. Acta*, 2014, **115**, 109-115.

42. Z. Dursun and B. Gelmez, *Electroanalysis*, 2010, **22**, 1106-1114.

43. S. Pruneanu, A. R. Biris, F. Pogacean, M. Coros, G. K. Kannarpady, F. Watanabe and A. S. Biris, *Electrochim. Acta*, 2014, **139**, 386-393.

44. X. Wang, M. Wu, W. Tang, Y. Zhu, L. Wang, Q. Wang, P. He and Y. Fang, *J. Electroanal. Chem.*, 2013, **695**, 10-16.

45. L. Yang, D. Liu, J. Huang and T. You, *Sensor Actuat. B-Chem*, 2014, **193**, 166-172.

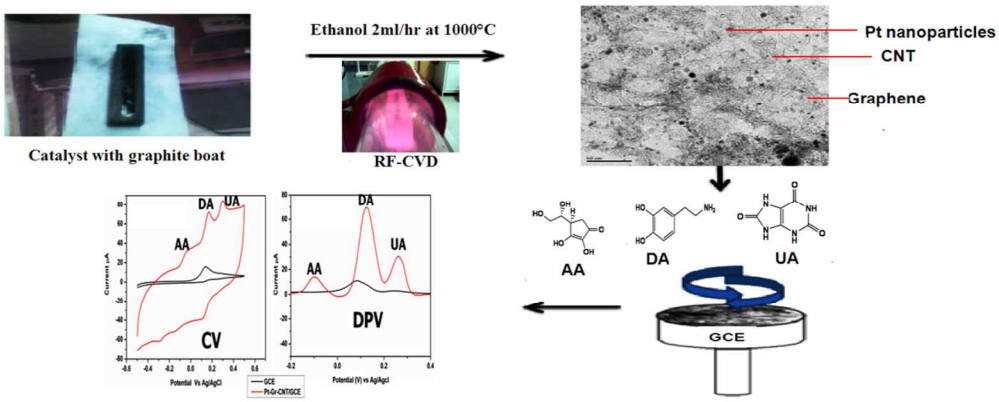

351x140mm (96 x 96 DPI)